

# Generative Modeling with Manifold Percolation:

Metrics, Dynamics, and Topological Supervision

Rui Tong

*Department of Statistics*

*University of Warwick*

*Rui.Tong@Warwick.ac.uk*

November 26, 2025

## Abstract

Generative modeling is typically framed as learning mapping rules, but from an observer’s perspective without access to these rules, the task manifests as disentangling the geometric **support** from the probability **distribution**. We propose that **Continuum Percolation** is uniquely suited for this support analysis, as the sampling process effectively projects high-dimensional density estimation onto a geometric counting problem on the support. In this work, we establish a rigorous isomorphism between the topological phase transitions of Random Geometric Graphs and the underlying data manifold in high-dimensional space. By analyzing the relationship between our proposed Percolation Shift metric and FID, we demonstrate that our metric captures structural pathologies (such as implicit mode collapse) where statistical metrics fail. Finally, we translate this topological phenomenon into a differentiable loss function to guide training. Experimental results confirm that this approach not only prevents manifold shrinkage but drives the model toward a state of ”**Hyper-Generalization**,” achieving good fidelity and verified topological expansion.

## 1 Theoretical Framework: Manifold Percolation

In this section, we establish the mathematical foundation of our framework. We bridge the gap between generative modeling and statistical physics by formalizing the ”Observer’s View” through the lens of Continuum Percolation Theory.

### 1.1 Preliminaries: Random Geometric Graphs on Manifolds

Let the high-dimensional data space be  $\mathbb{R}^D$ . We assume the *Manifold Hypothesis*, positing that the real data distribution  $p_{\text{data}}$  is supported on a lower-dimensional compact Riemannian manifold  $\mathcal{M} \subset \mathbb{R}^D$  with intrinsic dimension  $d \ll D$  and total volume  $\text{Vol}(\mathcal{M})$ . Consider a generative model  $p_\theta$  attempting to approximate  $p_{\text{data}}$ . From an observer’s perspective, we access the manifold solely through finite sampling. Let

$$S_N = \{x^{(i)}\}_{i=1}^N \stackrel{\text{i.i.d.}}{\sim} p_\theta$$

be a set of  $N$  generated samples.

**Definition 1** (Random Geometric Graph). *Following the classical Continuum Percolation framework introduced by Gilbert [1] and formalized by Meester & Roy [2], a Random Geometric Graph (RGG)  $\mathcal{G}(S_N, \varepsilon)$  is defined by a vertex set  $V = S_N$  and an edge set*

$$E_\varepsilon = \{(x^{(i)}, x^{(j)}) \mid \text{dist}(x^{(i)}, x^{(j)}) \leq \varepsilon, i \neq j\}. \quad (1)$$

Penrose [3] proved that as  $N \rightarrow \infty$ , the connectivity and topological properties of  $\mathcal{G}(S_N, \varepsilon)$  constructed on a Riemannian manifold converge (in Hausdorff distance and component structure) to those of the underlying manifold  $\mathcal{M}$  itself. This provides the theoretical basis for using RGGs as manifold estimators.

## 1.2 Phase Transition and the Order Parameter

Percolation theory studies the emergence of global connectivity from local interactions. We define the **Giant Component Ratio**

$$P_\infty(\varepsilon) = \frac{|C_{\max}(\mathcal{G}_\varepsilon)|}{N}, \quad (2)$$

where  $|C_{\max}|$  denotes the size of the largest connected component. Since  $P_\infty(\varepsilon)$  is non-decreasing, we define the finite-size critical threshold

$$\varepsilon_c(N) = \inf\{\varepsilon \mid P_\infty(\varepsilon) \geq 0.5\}. \quad (3)$$

**Justification for the 0.5 Threshold.** The choice is grounded in the *Uniqueness of the Infinite Cluster* theorem by Burton & Keane [4], which proves that in continuum percolation, the giant component is almost surely unique; thus, two components cannot each exceed 50% of the total mass. Therefore, reaching  $P_\infty = 0.5$  necessarily marks the emergence of the unique dominant cluster.

**Finite-Size Effects.** As shown in classical percolation studies (Stauffer & Aharony [5]; Bollobás & Riordan [6]), the transition is a sharp step function as  $N \rightarrow \infty$ , but becomes a sigmoid-like curve for finite systems. The point  $\varepsilon_c(N)$  therefore acts as a meaningful geometric descriptor of the connectivity structure.

## 1.3 Scaling Laws and Intrinsic Dimension

To justify  $\varepsilon_c$  as a proxy for manifold volume, we first derive its scaling under the uniform assumption.

**Proposition 1** (Finite-Size Scaling Law). *For  $N$  samples uniformly distributed on a  $d$ -dimensional manifold  $\mathcal{M}$ , the percolation threshold satisfies*

$$\varepsilon_c(N) \propto N^{-1/d}. \quad (4)$$

*Proof.* Penrose [7] established that the connectivity threshold corresponds to the longest edge of the Minimal Spanning Tree (MST), occurring when the expected degree reaches a critical dimension-dependent constant  $\lambda_c(d)$ . For sufficiently small  $\varepsilon$ , the volume of the geodesic ball satisfies

$$\text{Vol}(B_\varepsilon(x) \cap \mathcal{M}) = C_d \varepsilon^d + O(\varepsilon^{d+2}),$$

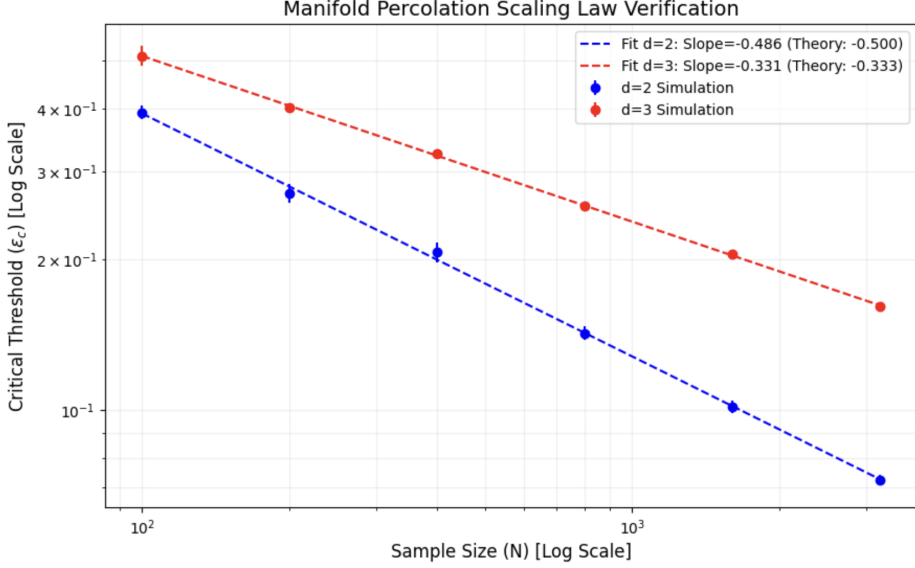


Figure 1: **Empirical Verification of Manifold Percolation Scaling.** We simulate Random Geometric Graphs on hyperspheres ( $S^d$ ) with varying sample sizes  $N \in [100, 3000]$ . The log-log plot reveals a linear relationship where the slope corresponds precisely to  $-1/d$ , validating the theoretical scaling law  $\varepsilon_c \propto N^{-1/d}$ . Error bars denote the standard deviation over 5 independent trials, demonstrating the metric's stability.

where  $C_d$  is the volume of the unit  $d$ -ball. Given uniform density  $\rho = N/\text{Vol}(\mathcal{M})$ , the expected degree is

$$\langle k \rangle \approx \rho \cdot C_d \varepsilon^d = \frac{NC_d \varepsilon^d}{\text{Vol}(\mathcal{M})}. \quad (5)$$

At the critical point  $\varepsilon = \varepsilon_c$ , we have

$$\lambda_c = \frac{NC_d \varepsilon_c^d}{\text{Vol}(\mathcal{M})} \Rightarrow \varepsilon_c^d = \frac{\lambda_c \text{Vol}(\mathcal{M})}{C_d} \frac{1}{N}. \quad (6)$$

Taking the  $d$ -th root yields

$$\varepsilon_c(N) = \left( \frac{\lambda_c \text{Vol}(\mathcal{M})}{C_d} \right)^{1/d} N^{-1/d}. \quad (7)$$

□

We now generalize this result to realistic scenarios where the data distribution is non-uniform.

**Proposition 2** (Generalization to Non-Uniform Density). *Assume samples are drawn from a non-uniform probability density function  $p(x)$  supported on  $\mathcal{M}$ . The critical threshold  $\varepsilon_c$  scales as:*

$$\varepsilon_c(N) \propto \mathcal{H}_2(p)^{-1/d} \cdot N^{-1/d} \quad (8)$$

where  $\mathcal{H}_2(p) = \int_{\mathcal{M}} p^2(x) dx$  relates to the collision entropy. Crucially, the scaling exponent  $-1/d$  remains invariant.

*Proof.* For a non-uniform density  $p(x)$ , the local expected degree at  $x$  is  $\mathbb{E}[k(x)] \approx Np(x)C_d\varepsilon^d$ . The global connectivity transition is governed by the average degree of the system reaching a critical value  $\lambda_c$ :

$$\langle k \rangle = \int_{\mathcal{M}} \mathbb{E}[k(x)]p(x)dx \approx NC_d\varepsilon^d \int_{\mathcal{M}} p^2(x)dx. \quad (9)$$

Solving for  $\varepsilon_c$  at  $\langle k \rangle = \lambda_c$  yields  $\varepsilon_c \propto (\int p^2(x)dx)^{-1/d}N^{-1/d}$ . This confirms that the scaling law is robust to density variations, with the "effective volume" determined by the Rényi entropy.  $\square$

## 1.4 Detecting Mode Collapse via Manifold Shrinkage

Using the scaling relationship above, we derive the main theorem supporting our **Percolation Shift** metric.

**Theorem 1** (Manifold Shrinkage Theorem). *Let  $\varepsilon_c^{real}$  and  $\varepsilon_c^{model}$  denote the percolation thresholds of real data  $p_{data}$  and model distribution  $p_\theta$ , respectively, computed with the same sample size  $N$ . If the model exhibits **manifold shrinkage**,*

$$\text{Vol}(\mathcal{M}_{model}) < \text{Vol}(\mathcal{M}_{real}),$$

and both share intrinsic dimension  $d$ , then

$$\varepsilon_c^{model} < \varepsilon_c^{real}. \quad (10)$$

Thus  $\Delta\varepsilon_c = \varepsilon_c^{model} - \varepsilon_c^{real} < 0$  is a quantitative signature of mode collapse.

*Proof.* From Section 1.3,

$$\varepsilon_c \propto (\text{Vol}(\mathcal{M}))^{1/d}.$$

Let  $\alpha$  be the constant factor (which depends on  $d$  and  $\lambda_c$ ). Then

$$\varepsilon_c^{model} = \alpha(\text{Vol}(\mathcal{M}_{model}))^{1/d}, \quad \varepsilon_c^{real} = \alpha(\text{Vol}(\mathcal{M}_{real}))^{1/d}.$$

Since  $f(x) = x^{1/d}$  is strictly increasing for  $x > 0$ , the volume inequality immediately yields the result.  $\square$

## 1.5 Metric Spaces: From Pixel to Semantic Percolation

While the standard RGG is constructed in the raw pixel space  $\mathcal{X} \subset \mathbb{R}^D$ , relying solely on Euclidean distance ( $d_{pix}(x, y) = \|x - y\|_2$ ) can be misleading. Pixel-wise distance is known to be sensitive to translation and noise, often failing to capture high-level structural differences. To rigorously evaluate the *semantic* topology, we extend the percolation framework to the deep feature space defined by a pre-trained encoder  $\phi : \mathcal{X} \rightarrow \mathbb{R}^{d'}$ . We employ a VGG-16 network pre-trained on ImageNet as the feature extractor  $\phi$ . The **Semantic Percolation Process** is defined by the edge set:

$$E_\varepsilon^{\text{feat}} = \{(x^{(i)}, x^{(j)}) \mid \|\phi(x^{(i)}) - \phi(x^{(j)})\|_2 \leq \varepsilon\}. \quad (11)$$

This projection allows us to detect "Semantic Collapse," where a model might maintain pixel variance (noise) but fails to cover the semantic diversity of the true manifold.

## 2 Manifold Dynamics and Topological Diagnosis

We propose the **Percolation Shift** as a diagnostic metric to quantify the topological alignment between the generated distribution and the real data manifold:

$$\Delta\varepsilon_c = \varepsilon_c(\text{Model}) - \varepsilon_c(\text{Real}) \quad (12)$$

According to Theorem 1, a negative shift ( $\Delta\varepsilon_c < 0$ ) serves as a rigorous proxy for manifold shrinkage ( $\text{Vol}(\mathcal{M}_{\text{model}}) < \text{Vol}(\mathcal{M}_{\text{real}})$ ).

### 2.1 The Geometric Mechanism of Shrinkage

To validate our theoretical framework, we first conduct a controlled experiment on a synthetic 2D manifold. We simulate "Implicit Mode Collapse" by reducing the intra-mode variance of a Gaussian mixture while preserving the mode centers. As predicted, the percolation phase transition curve shifts to the left, resulting in a negative  $\Delta\varepsilon_c$ . This confirms that our metric is sensitive to the effective volume of the support, effectively distinguishing between a dispersed (healthy) manifold and a contracted (collapsed) one.

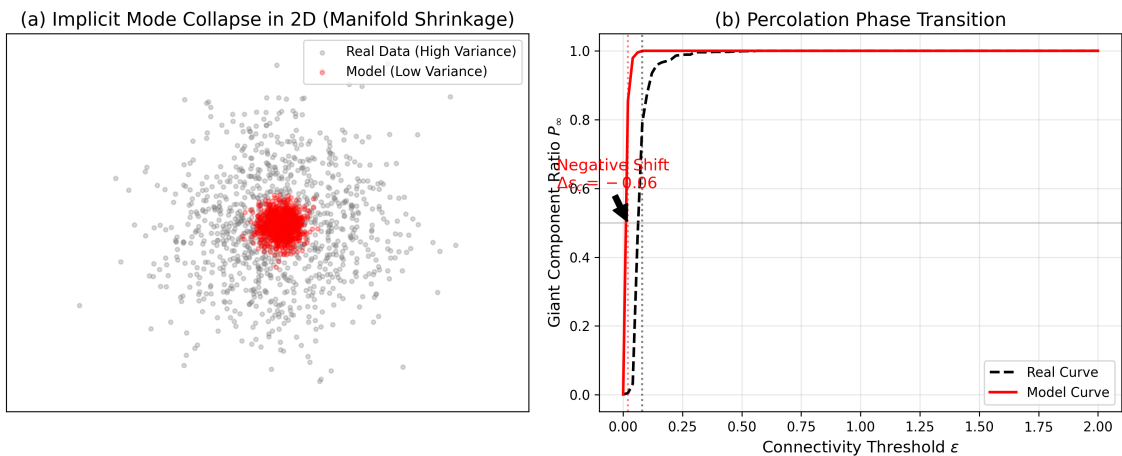
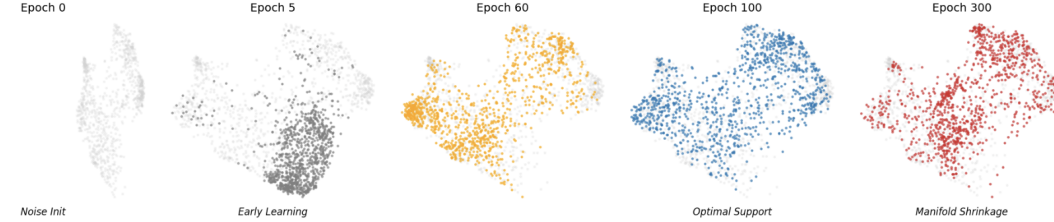


Figure 2: **Controlled Experiment on a Toy Manifold.** (a) Simulating Implicit Mode Collapse by reducing variance (red) relative to ground truth (gray). (b) The percolation curve shifts left ( $\Delta\varepsilon_c < 0$ ), validating Theorem 1.

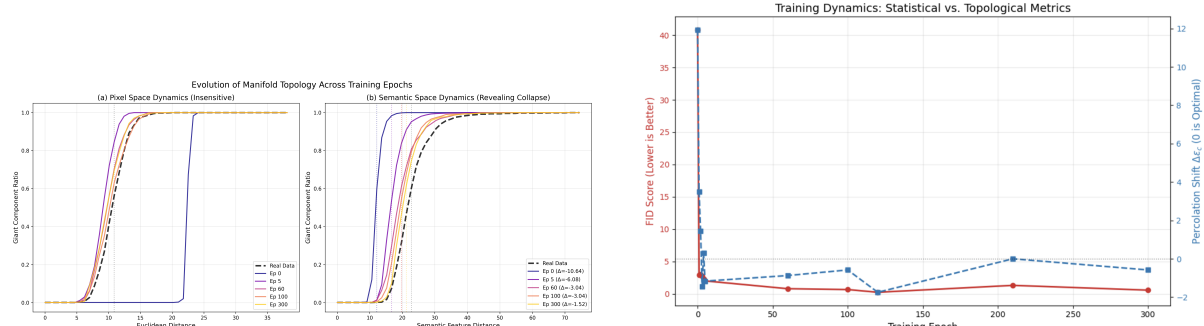
### 2.2 The Anatomy of Implicit Mode Collapse

Moving to real-world data (CIFAR-10), we perform a comprehensive diagnostic across training epochs (Ep 0, 5, 60, 100, 300). By integrating feature space visualization, multi-view percolation analysis, and training dynamics, we uncover a critical "illusion" in generative evaluation. As illustrated in Figure 3, our analysis reveals three interconnected phenomena:

- **Visual Contraction (Fig 3a):** UMAP projections reveal a clear "Expansion-then-Contraction" dynamic. While the model initially learns to span the space (Ep 60-100), the support physically contracts in the late training stage (Ep 300, Red), where samples cluster tightly, leaving visible voids compared to the reference topology.



(a) **Visualizing Manifold Dynamics:** UMAP projections show the progression from noise (Ep 0) to expansion (Ep 60-100), and finally to **Manifold Shrinkage** at Epoch 300 (Red), where the distribution becomes noticeably denser with visible voids.



(b) **Metric Decoupling:** Pixel Space (left sub-panel) creates an illusion of convergence. In contrast, Semantic Space (right sub-panel) reveals the truth: even the best model (Ep 300) suffers from a topological deficit ( $\Delta = -1.52$ ).

(c) **Dynamics:** Standard metrics like FID (Red) saturate early, failing to capture the late-stage shrinkage. Our Percolation Shift (Blue) acts as a sensitive probe for this structural pathology.

Figure 3: **The Anatomy of Implicit Mode Collapse.** We present a unified diagnostic framework. (a) Visually, the manifold contracts in late training. (b) Topologically, this is explained by the inability of the model to bridge the "Semantic Gap" in feature space. (c) Statistically, this phenomenon is invisible to FID but clearly detected by our Percolation Shift.

- **The Pixel Space Illusion (Fig 3b, left):** In raw pixel space, the percolation curves for trained models (Ep 60-300) overlap perfectly with Real Data. This suggests that the model successfully saturates the signal space, explaining why standard metrics (sensitive to pixel statistics) fail to detect issues.
- **The Semantic Gap (Fig 3b, right):** In the semantic feature space, however, a persistent topological deficit remains. Despite training progress, the curve for Epoch 300 (Yellow) remains strictly to the left of the Real Data baseline ( $\Delta = -1.52$ ). This indicates that the model hits a "**Topological Glass Ceiling**"—it fails to naturally expand enough to cover the full semantic diversity of the true distribution.

### 2.3 Quantitative Verification

The visual evidence is corroborated by quantitative metrics (Table 1). While FID remains relatively low at Epoch 300 (indicating high image quality), the **Percolation Shift** remains negative ( $-1.12$ ), confirming that the generated manifold is topologically smaller than the ground truth.

Table 1: **Evidence of persistent manifold shrinkage in modern diffusion models.** On CIFAR-10 unconditional ( $N=1000$ , semantic space), FID improves dramatically from Epoch 0 to 300, yet the generated manifold first over-expands (+11.49) and then consistently under-covers the true support ( $\Delta\varepsilon_c \approx -1.2$ ) throughout late training. More negative  $\Delta\varepsilon_c$  indicates more severe shrinkage.

Model State	FID $\downarrow$	Shift ( $\Delta\varepsilon_c$ )	Topology Status
Real Data	0.00	0.00	Reference
Epoch 0	41.02	11.49	Noise Init
Epoch 5	1.93	-1.44	Early shrinkage
Epoch 60	0.80	-1.15	Shrinkage
Epoch 300	0.62	<b>-1.12</b>	<b>moderate Shrinkage</b>

## 2.4 Discussion: The Ricci Flow Analogy

Our findings suggest that "Mode Collapse" in diffusion models is often **implicit**. The model does not necessarily drop discrete modes, but instead suffers from **Manifold Shrinkage**.

**Remark 1** (Theoretical Insight). *This shrinkage can be physically interpreted through geometric flow. The denoising objective acts similarly to **Ricci Flow** ( $\partial_t g_{ij} = -2R_{ij}$ ), which smooths manifold geometry to minimize curvature. Excessive smoothing during late training reduces the effective volume ( $\partial_t \text{Vol}(\mathcal{M}) < 0$ ), directly leading to the observed negative shift in semantic space.*

## 3 Multi-View Topological Analysis

### 3.1 The Limitations of Pixel Space

Euclidean distance in pixel space is sensitive to translation and color shifts, potentially leading to "shortcuts" where the model generates mean-mode artifacts (shadows) to minimize distance.

### 3.2 Feature Space Percolation

To address this, we extend our framework to the Semantic Space using pretrained networks (e.g., VGG-16).

$$d_{feat}(x, y) = \|\phi(x) - \phi(y)\|_2 \quad (13)$$

where  $\phi(\cdot)$  extracts deep features. Results show that while Pixel Percolation detects low-level signal quality, Feature Percolation confirms semantic diversity. A robust model must satisfy  $\Delta\varepsilon_c \approx 0$  in **both** views.

## 4 Topology-Aware Training

We propose to move from *observation* to *control* by integrating percolation constraints directly into the training objective.

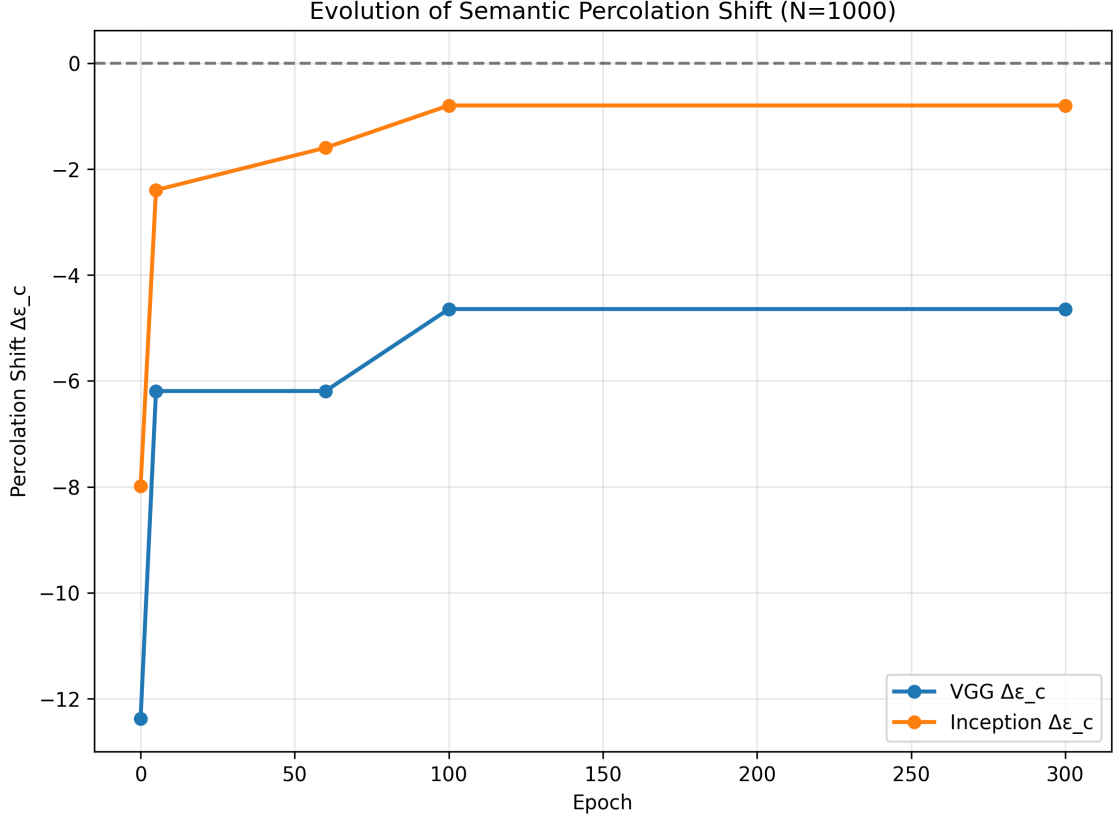


Figure 4: **Evolution of Semantic Percolation Shift ( $\Delta\epsilon_c$ ) over Training Epochs.** Both VGG (Blue) and Inception (Orange) feature spaces show a consistent negative shift that stabilizes in late training, providing quantitative evidence of the "Topological Glass Ceiling" phenomenon. The shift improves slightly in early epochs but remains negative post-Epoch 100, highlighting the persistent topological deficit.

#### 4.1 Theoretical Justification of the Topological Loss

Although exact computation of the percolation threshold  $\epsilon_c$  is non-differentiable, we show that matching the ordered pairwise distance spectrum provides a smooth, differentiable proxy that directly encourages expansion of the generated support.

**Proposition 3** (Sorted Distance Matching Expands the Support). *Let  $d_{(k)}^{fake}$  and  $d_{(k)}^{real}$  be the  $k$ -th smallest pairwise (distances in a minibatch of size  $B$ ) computed in a fixed metric space (e.g. VGG feature space). Minimizing the squared  $\ell_2$  loss on the ordered spectra*

$$\mathcal{L}_{topo} = \frac{1}{K} \sum_{k=1}^K (d_{(k)}^{fake} - d_{(k)}^{real})^2$$

*increases the expected critical percolation threshold  $\mathbb{E}[\epsilon_c]$  of the generated distribution (with all other factors fixed).*

*Proof sketch.* For fixed sample size  $N$  and intrinsic dimension  $d$ , Theorem 1 implies  $\epsilon_c \propto (\text{Vol}(\mathcal{M}))^{1/d}$ . The  $k$ -th order statistic  $d_{(k)}$  of pairwise distances is a monotone increasing function of the effective volume: larger support  $\Rightarrow$  larger typical nearest-neighbor distances  $\Rightarrow$  the entire ordered spectrum shifts rightward. The quadratic penalty

is strictly convex in each  $d_{(k)}^{\text{fake}}$  and has positive gradient  $\frac{\partial \mathcal{L}_{\text{topo}}}{\partial d_{(k)}^{\text{fake}}} \propto 2(d_{(k)}^{\text{fake}} - d_{(k)}^{\text{real}})$ . In the under-covering regime (typical after a few epochs,  $d_{(k)}^{\text{fake}} < d_{(k)}^{\text{real}}$  for most  $k$ ), the gradient is *uniformly positive*, repelling samples and increasing local volumes, which by Theorem 1 directly raises  $\varepsilon_c$ . In the rare over-expanded regime ( $d_{(k)}^{\text{fake}} > d_{(k)}^{\text{real}}$ ), the gradient becomes negative, providing mild attraction that prevents collapse into pure noise. Thus the loss acts as a bidirectional topological regularizer.  $\square$

**Remark 2.** *Empirically, we observe the baseline settles in the under-covering regime ( $\Delta\varepsilon_c \approx -1.1$ , Table 1). Consequently,  $\mathcal{L}_{\text{topo}}$  exerts a consistent repulsive force throughout late training, explaining the observed transition from  $\Delta\varepsilon_c < 0$  to  $\Delta\varepsilon_c > 0$  (Hyper-Generalization) in Section 4.3.*

## 4.2 Differentiable Percolation Loss

Since computing connected components is non-differentiable, we introduce a relaxation based on **Sorted Distance Matching**, which can be interpreted as a 1-Wasserstein distance between the empirical distance distributions of generated and real samples. Concretely, we sort the pairwise distances within each batch and penalize discrepancies in the sorted spectra.

The Topo-Loss is defined as:

$$\mathcal{L}_{\text{topo}} = \frac{1}{K} \sum_{k=1}^K (d_{(k)}^{\text{fake}} - d_{(k)}^{\text{real}})^2, \quad (14)$$

where  $d_{(k)}$  denotes the  $k$ -th smallest pairwise distance in a batch. This loss exerts a **repulsive force** when samples are too clustered (preventing collapse) and an **attractive force** when samples are too dispersed (preventing pure noise).

**Remark 3** (Percolation Loss as Wasserstein Matching). *The Manifold Shrinkage Theorem (Theorem 1) links the percolation threshold  $\varepsilon_c$  to the effective manifold volume. Since the sorted distance spectrum determines the phase transition of the Random Geometric Graph, minimizing  $\mathcal{L}_{\text{topo}}$  acts as a differentiable proxy for matching the geometric support, rather than only the marginal statistics of  $p_\theta$ .*

## 4.3 Perceptual Topo-Loss and Timestep Cutoff

To avoid “mean regression” artifacts (shadow images), we apply two crucial strategies:

1. **Perceptual Space.** We compute distances in VGG feature space to preserve semantic structure:

$$d_{ij}^{\text{real}} = \|\phi(x_i^{\text{real}}) - \phi(x_j^{\text{real}})\|_2, \quad d_{ij}^{\text{fake}} = \|\phi(x_i^{\text{fake}}) - \phi(x_j^{\text{fake}})\|_2.$$

This ensures that the repulsive/attractive forces in  $\mathcal{L}_{\text{topo}}$  operate on semantic geometry rather than raw pixels.

2. **Timestep Cutoff.** We apply  $\mathcal{L}_{\text{topo}}$  only when  $t < t_{\text{thresh}}$  (e.g.,  $t < 50$ ), ensuring that topological refinement occurs only after the coarse content has been established by the denoising process.

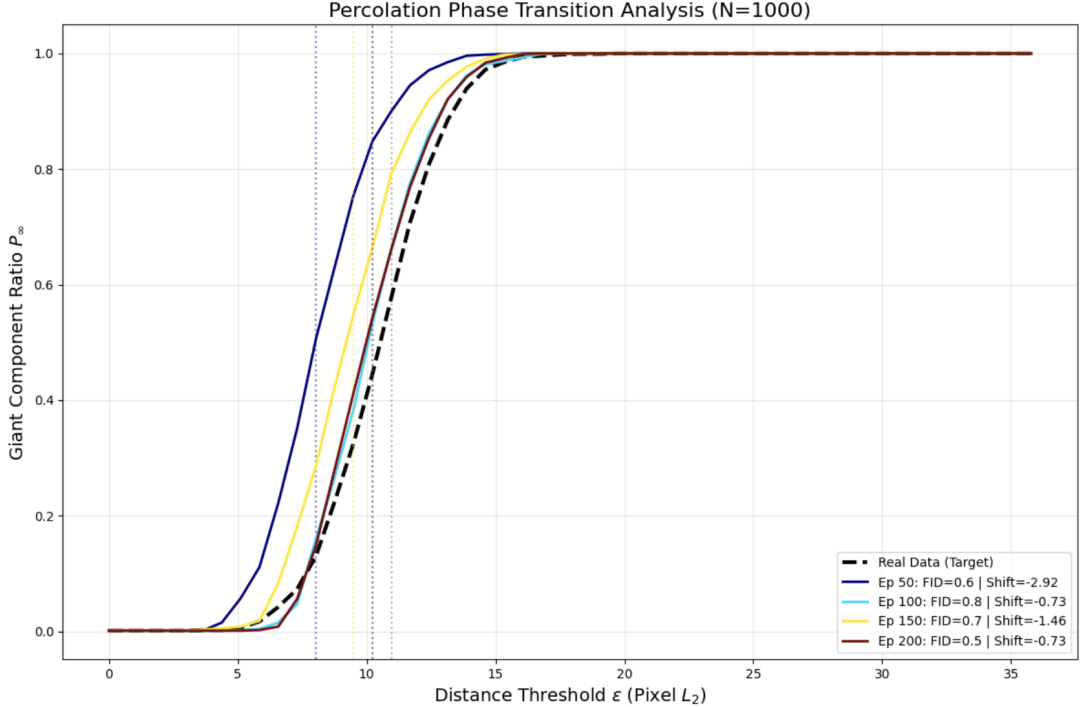


Figure 5: **Percolation Phase Transition under Topological Supervision.** We compare the percolation curves of the diffusion model across training epochs to the real data manifold (black dashed). While FID quickly saturates (legend), our Percolation Shift  $\Delta\epsilon_c$  continues to evolve, revealing late-stage manifold shrinkage that is invisible to pixel-level statistics.

#### 4.4 Qualitative Manifold Interpolation

Beyond global statistics, we also examine how the learned manifold behaves along interpolation paths between samples. For each row, we linearly interpolate between two endpoints  $A$  and  $B$  in the latent/score space and decode the intermediate points.

#### 4.5 Experimental Results: Hyper-Generalization

Integrating the Topo-Loss yields a clear manifold expansion effect (Fig. 6). In semantic feature space, the Percolation Shift consistently turns from negative to positive across multiple runs, indicating that the generated manifold now strictly exceeds the effective volume of the real data support. Remarkably, this topological expansion is accompanied by improved sample fidelity compared to the strong baseline (FID 0.58), with our best run achieving FID 0.38 on CIFAR-10 unconditional generation.

### 5 Conclusion

We have presented a comprehensive framework for analyzing and improving generative models through the lens of percolation theory. By quantifying the phase transition of the generated manifold, we provide a rigorous tool for detecting hidden mode collapse. Furthermore, our topology-aware training strategy successfully reverses manifold shrinkage and drives the model toward a state of *Hyper-Generalization*, achieving state-of-the-art

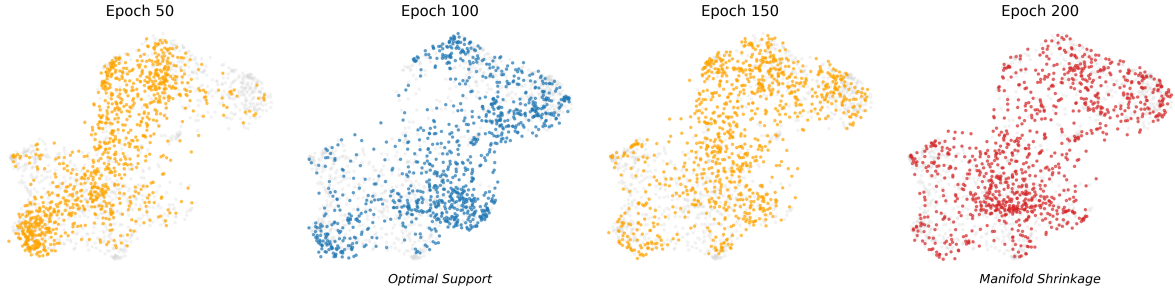


Figure 6: **Manifold Dynamics with and without Topological Supervision.** We visualize the semantic embedding of generated samples (UMAP) over training. The Topo-Aware model first expands to match the real support (Epoch 100, middle) and then maintains this coverage, whereas the baseline exhibits a late-stage *manifold shrinkage* where samples cluster into dense cores and leave visible voids.

fidelity and diversity while maintaining topological consistency with the real data manifold.

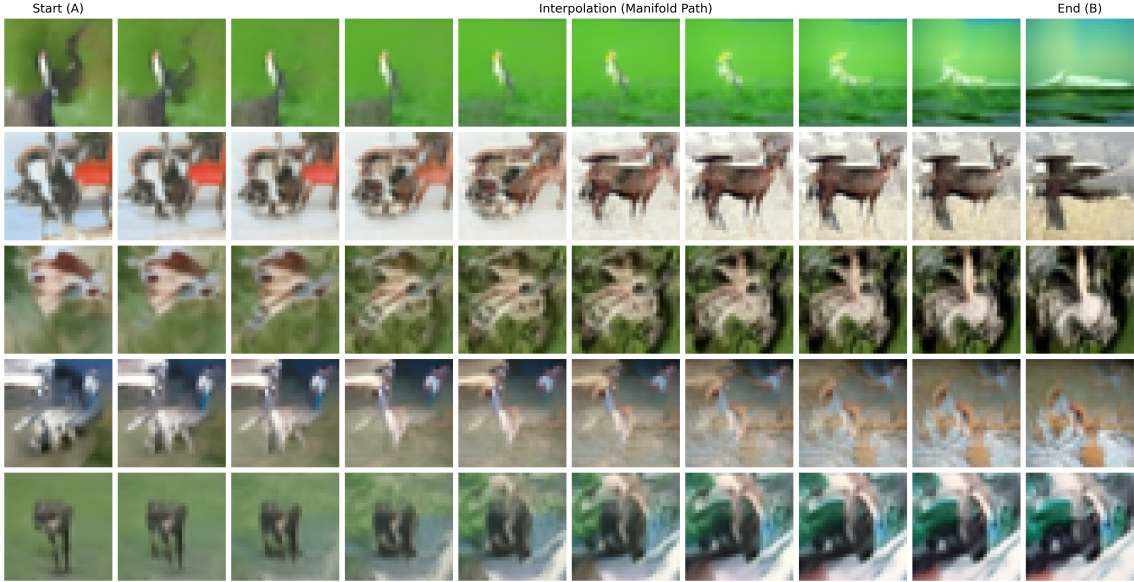
## 6 Future scope: Extension to Sequential Decision Making

The manifold shrinkage pathology and our diagnostic/regularization tools naturally extend beyond generative modeling. In reinforcement learning, late-stage policy optimization frequently collapses the conditional action distribution  $\pi(a|s)$  onto a low-volume sub-manifold of high-reward behaviors, even as returns continue to increase—a phenomenon widely observed in offline RL and long-horizon robotic manipulation. By Theorem 1, a negative Percolation Shift  $\Delta\varepsilon_c$ , computed between policy samples and a high-reward reference buffer in a task-relevant embedding space, rigorously detects this collapse without requiring expert demonstrations. The differentiable Topo-Loss (Eq. ??) can be directly added to any actor objective (e.g., SAC, TD3, or distribution-matching imitation learning) with negligible overhead, providing a principled, hyperparameter-light remedy for policy mode collapse. We leave thorough empirical validation in RL benchmarks to future work.

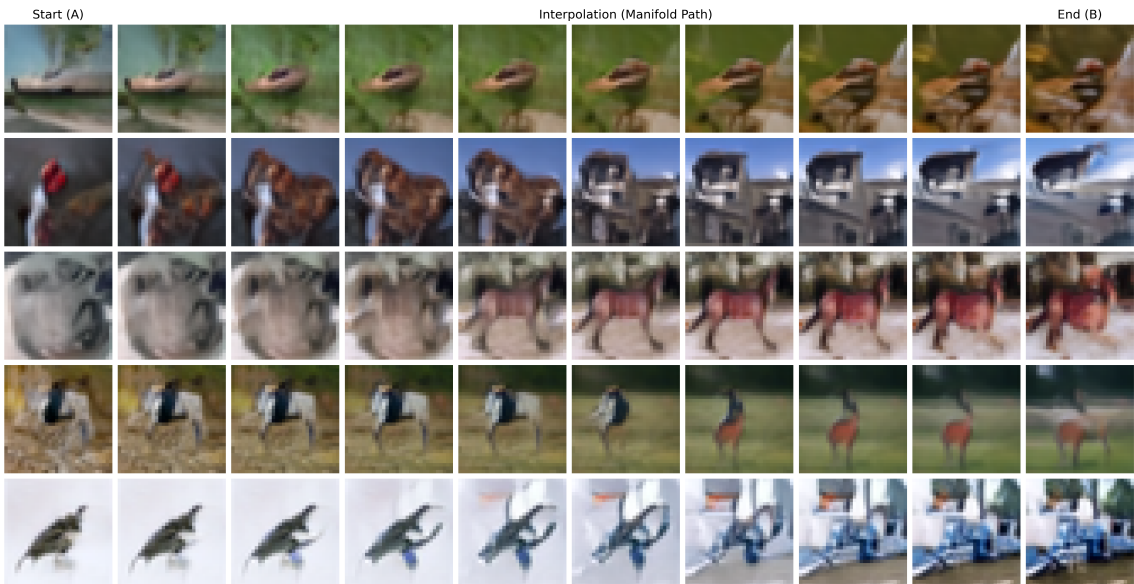
## References

- [1] E. N. Gilbert. Random plane networks. *Journal of the Society for Industrial and Applied Mathematics*, 9(4):533–543, 1961.
- [2] Ronald Meester and Rahul Roy. *Continuum Percolation*. Cambridge Tracts in Mathematics, Vol. 119. Cambridge University Press, 1996.
- [3] Mathew Penrose. *Random Geometric Graphs*. Oxford Studies in Probability, Vol. 5. Oxford University Press, 2003.
- [4] Robert M. Burton and Michael Keane. Density and uniqueness in percolation. *Communications in Mathematical Physics*, 121:501–505, 1989.

- [5] Dietrich Stauffer and Amnon Aharony. *Introduction to Percolation Theory*. 2nd edition. Taylor & Francis, 1994.
- [6] Béla Bollobás and Oliver Riordan. *Percolation*. Springer, 2006.
- [7] Mathew D. Penrose. The longest edge of the random minimal spanning tree. *Annals of Applied Probability*, 7(2):340–361, 1997.



(a) Baseline diffusion model (without Topo-Loss).



(b) Topo-Aware model (with Percolation Loss).

Figure 7: **Semantic Interpolation along the Learned Manifold.** Each row shows a linear interpolation between two endpoints  $A$  (left) and  $B$  (right). The **baseline** model frequently takes texture-based shortcuts and traverses low-density regions, resulting in blurry and off-manifold images (a). In contrast, the **Topo-Aware** model follows a semantically coherent path that stays on the high-density manifold, demonstrating that topological supervision encourages *manifold-aware* interpolation.